MEMS-Based Nanospray-Ionization Mass Spectrometer

Steven Wright, Richard R. A. Syms, *Senior Member, IEEE*, Richard Moseley, Guodong Hong, Shane O'Prey, William E. Boxford, Neil Dash, and Peter Edwards

***Abstract*—An electrospray-ionization mass spectrometer (ESI-MS) whose main components are all fabricated using silicon microelectromechanical systems (MEMS) techniques is demonstrated for the first time. The ion source consists of a micro-engineered alignment bench containing a V-groove mounting for a nanospray capillary, an ion-extraction electrode, and a pneumatic nebulizer. The vacuum interface consists of two plates, each carrying a 50-μm-diameter capillary, that are selectively etched and bonded together to provide a differentially pumped internal cavity. The quadrupole filter consists of a microfabricated frame that provides mountings for stainless-steel rods measuring 650 μm in diameter and 30 mm in length. Two different quadrupoles are compared: a first-generation bonded silicon device and a second-generation silicon-on-glass device with a Brubaker prefilter. Differential pumping of a MEMS component is demonstrated for the first time, atmospheric pressure ionization and ion transfer into vacuum are characterized, ESI-MS operation is demonstrated, and spectra are presented for a variety of compounds. [2010-0108]**

***Index Terms*—Electrospray, mass spectrometry, microelectromechanical systems (MEMS), quadrupole filter.**

I. Introduction

OVER 25 YEARS have passed since an electrospray-ionization (ESI) source was first coupled to a quadrupole mass spectrometer (MS) by Yamashita and Fenn [1]. Since then, ESI-MS has become a workhorse of analytical chemistry, allowing analytes to be ionized at atmospheric pressure with little fragmentation and passed into a vacuum system for analysis.

Conventional ESI sources employ spray tips with an internal diameter (ID) of ≈ 100 μm [2]. In order to establish a Taylor cone and maintain stable emission of charged droplets, minimum flow rates of 0.5–5 $\mu\mathrm{L}\cdot\mathrm{min}^{-1}$ and voltages of 2.5–4 kV are used. However, it has been convincingly demonstrated that high sensitivity and stable emission can be achieved at much lower flow rates and voltages using spray tips with IDs of ≈ 5 μm, and silica nanospray capillaries with a range of coatings have become widely available [3]–[8]. Unfortunately, while these are inexpensive, operator expertise and costly positioning apparatus are often required for stable and reproducible performance.

Electrosprayed ions are passed into a low-pressure chamber via a vacuum interface. The simplest interface is a single orifice or capillary that allows gas and entrained ions to pass directly into the vacuum chamber. Clearly, the orifice must be small enough or the pumps large enough to ensure that the pressure is consistent with mass analysis. However, the susceptibility of very small orifices to clogging and the inconvenience of large pumps led to this approach being abandoned. Modern instruments employ one or more stages of differential pumping. Larger orifices can be tolerated since only a fraction of the flow is transmitted to the vacuum chamber, while majority of the gas load can be pumped away at higher pressure using more modest pumps.

The effective transfer of ions and molecules from atmospheric pressure into vacuum involves a shock-free supersonic expansion, whose principles have been applied to many different applications and dimensional scales. Work on rocket engines during and immediately after the Second World War led to an early understanding of flow in Laval nozzles [9], [10]. Following a suggestion by Kantrowitz and Grey, supersonic expansion was adopted for use in intense molecular beam sources (see, e.g., [11]–[17] and summaries in [18], [19]) and then, later, for high-speed wind tunnels used for high-speed aircraft testing [20]. Similar methods were then applied to inductively coupled plasma MSs [21]–[26] and ESI-MS systems [1], [27]–[31]. In each case, many of the details of the complex shock phenomena involved have been verified by visual observation of flow patterns [13], [24], [26] or pressure measurements [25].

Multistage expansion conveys several benefits. First, beam collimation may be improved through a transfer of thermal energy to kinetic energy in the free-jet expansion that occurs as gas, and ions emerge from an orifice into a region of lower pressure. The expansion is terminated by a normal shock, known as a Mach disk; however, an intense collimated beam can be transmitted to the next stage by using a skimmer to pierce the Mach disk. Secondly, there is an opportunity in each stage to improve the ion density by using ion optical elements such as quadrupole ion guides [32], [33], wire ion guides [34], [35], stacked-ring ion guides [36], [37] or electrostatic discriminators [38] to transfer ions while neutrals are pumped away. Reviews of ESI-MS interfaces can be found in [39] and [40].

Relentless commercial development led to many improvements in sensitivity, ease of use, and functionality. However,

Manuscript received April 21, 2010; revised August 25, 2010; accepted August 26, 2010. Date of publication October 28, 2010; date of current version November 30, 2010. This work was supported in part by the Department of Trade and Industry under the Advanced Technology Project IONCHIP, by Merck & Company, by Pfizer Inc., and by GlaxoSmithKline plc. Subject Editor G. Stemme.

S. Wright, R. Moseley, G. Hong, S. O'Prey, W. E. Boxford, N. Dash, and P. Edwards are with Microsaic Systems Ltd., Surrey, GU21 5BX, U.K. (e-mail: swright@microsaic.com; rmoseley@microsaic.com; ghong@micosaic.com; soprey@microsaic.com; wboxford@microsaic.com).

R. R. A. Syms is with the Electrical and Electronic Engineering Department, Imperial College, London, SW7 2AZ, U.K. (e-mail: r.syms@imperial.ac.uk).

Digital Object Identifier 10.1109/JMEMS.2010.2082501

most modern ESI-MS instruments are still based on expensive precision-machined components and vacuum systems requiring large pumps. Increasingly, a different approach to the manufacture of components for mass spectrometry is being pursued through the use of microelectromechanical system (MEMS) technology.

The strongest interest has been in the integration of nanospray tips with microfluidic systems, such as capillary electrophoresis separators [41]–[45], which gives a direct analytical benefit in terms of reduced peak broadening. Most chip-based nano-ESI sources provide in-plane emission from closed channels, but variants emitting from surfaces or open channels exist [46]–[49], and emission can take place from 1-D in-plane or 2-D out-of-plane arrays [50]–[53]. Additional features such as pneumatic nebulizers have been incorporated to enhance emission [44], [54], [55]. Reviews of laboratory-on-a-chip nanoelectrospray sources can be found in [56]–[59].

The more difficult problem of miniaturizing mass filters has also been addressed, and interest is increasing rapidly as performance improves. Most common filter types have been fabricated using MEMS techniques. These include crossed-field [60]–[62] and traveling-wave [63]–[65] filters, time-of-flight analyzers [66]–[69], cylindrical ion traps [70]–[75], and linear [76]–[80] ion traps. However, quadrupole filters have so far offered the best performance in terms of mass range and mass resolution. In the earliest example, the rods were held in grooves created by crystal plane etching of bulk silicon [81], [82]. Although basic operation was demonstrated, resolution and mass range were both limited. A more successful filter, with a mass range of $m/z = 400$ and a resolution of $m/\Delta m = 80$ at 10% peak height, was developed by Microsaic Systems [83], [84] and used in complete benchtop systems [85]. The rods were supported in a silicon frame, fabricated by deep reactive ion etching (DRIE) of bonded silicon-on-insulator (BSOI) material. Using a similar approach but with an out-of-plane geometry, a mass range of $m/z = 614$ and an estimated resolution of $m/\Delta m \approx 13$ at 10% peak height was demonstrated at the Massachusetts Institute of Technology [86]. Recently, a new silicon-on-glass design from Microsaic Systems incorporating a prefilter achieved a mass range of $m/z = 1200$ and a resolution of $m/\Delta m \approx 150$ at 10% peak height [87]. Other approaches include the use of DRIE [88], [89] and rapid prototyping [90], [91] to form electrodes. Reviews of MEMS mass filters can be found in [92]–[95].

Vacuum interfaces are conspicuously absent from the list of components that have been realized in microfabricated form. As a result, the potential impact of miniaturization on the overall size of ESI-MS systems has been limited. In this paper, we introduce a low-cost vacuum interface constructed using silicon technology. We do not attempt to tackle the complicated problem of skimmer fabrication but instead show how a simple differentially pumped interface may be constructed. We then use it in conjunction with a MEMS nanospray-ionization source and two different MEMS quadrupole filters to demonstrate a complete ESI-MS system in which all the ion source, ion transmission, and mass filtering components are fabricated as silicon devices. The overall design of an ESI-MS system is first reviewed in Section II. The MEMS ESI-MS system and construction of all-silicon-based components is described in Section III. Operation of the MEMS ESI-MS system is demonstrated in Section IV, and the performance of the two mass filters is compared. Conclusions are drawn in Section V.

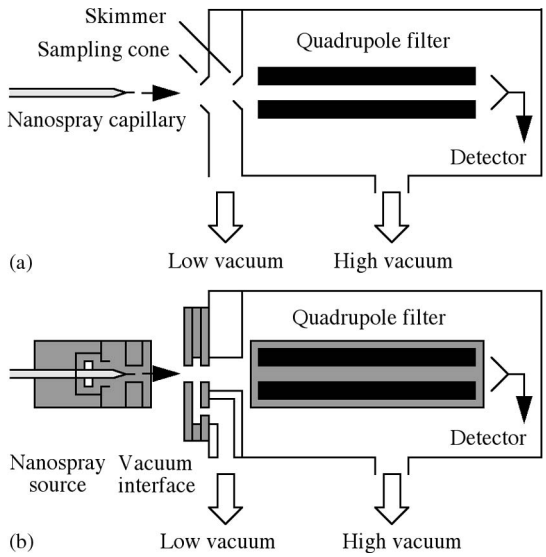

Fig. 1. ESI mass spectrometry systems implemented using (a) conventional and (b) (highlighted in gray) MEMS components. Each system consists of a nanospray source operating at atmospheric pressure, a differentially pumped interface, and a quadrupole mass filter and ion detector contained in a vacuum chamber.

II. ESI-MS Systems

In this Section, we briefly review the design of conventional ESI-MS systems, the operation of vacuum interfaces, and the issues accompanying interface miniaturization.

A. ESI-MS System Overview

Fig. 1(a) shows the main components of a conventional ESI-MS system. The source is a nanospray capillary, which derives its input from (for example) a liquid chromatograph or capillary electrophoresis separator. Spray is generated at atmospheric pressure using a voltage applied between the analyte and the input to the MS, which draws in ions through a sampling cone. Various methods are used to reduce the flow of neutrals and protect the system from large droplets and salt contamination, including the use of off-axis spray, a curtain gas, and dogleg or Z-shaped internal ion paths. Desolvation may be promoted by heating sections of the ion path. The space between the sampling cone and the skimmer is held at intermediate pressure by a high-capacity pump. In this region, ion optical components may be placed to concentrate ions (generally, by collision focusing) so that these are preferentially passed into the high-vacuum chamber. The mass analyzer may be one of the many types in common use, including (as shown here) a quadrupole filter.

Fig. 2 shows a conventional vacuum interface, which uses supersonic expansion to increase the average axial velocity of molecules and entrained ions. The process operates by trading thermal energy for kinetic energy, so the gas cools as it

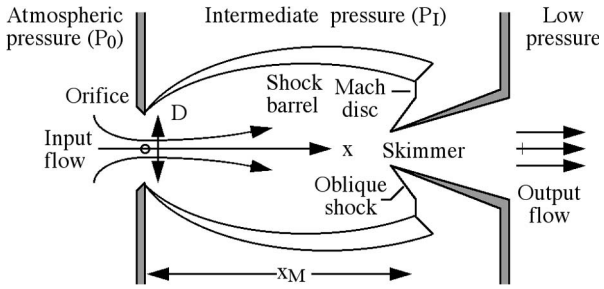

Fig. 2. Free-jet expansion in a conventional vacuum interface. The gray shaded parts indicate the ion sampling orifice and the skimmer cone. The lines indicate gas flow and the formation of a barrel shock in the intermediate chamber, terminated by a Mach disk anchored on the skimmer. D is the diameter of the input capillary; x_M is the distance to the Mach disk.

accelerates. The expected improvement in centerline flux over a simple effusive source (for equal orifice flows) is $\gamma M^2/2 + 3/2$. Here, $\gamma = C_P/C_V$ is the ratio of the specific heats at constant pressure and constant volume, and M is the Mach number, i.e., the ratio of the velocity to the local speed of sound. Since M may be 10–20, the potential improvement is very significant.

Full understanding of the gas-dynamics problem requires the solution of the Navier–Stokes equations for compressible flow in three dimensions. Until recently, this task was beyond existing computers. Analysis was therefore carried out using simpler theory and formulas with a good fit to available data. Pressure, temperature, density, and flow velocity are simply linked by the rules of adiabatic processes. Using these, it can be shown that a rising velocity is only obtained in a converging channel up to a speed of Mach 1. Above Mach 1, further increases in velocity are only obtained in a diverging nozzle, which then emits a supersonic jet. Other phenomena, such as shock waves, occur. Normal shocks are generated by rapid changes in pressure, and oblique shocks are generated by changes in boundaries or obstacles. Flow patterns are disturbed by oblique shocks, which, in extreme cases, scatter the flow.

B. Vacuum-Interface Operation

Free-jet expansion is a limiting case of a convergent–divergent nozzle in which the diverging section is omitted. The gas is initially stationary at atmospheric pressure P_0 and discharges into a chamber at an intermediate pressure P_I. Entering the orifice, the flow converges and accelerates, reaching Mach 1 near the exit. Leaving the orifice, it diverges. The pressure, density, and temperature decrease, and the Mach number increases. Combining adiabatic relations with the continuity equation, it can be shown (see, e.g., [19]) that M varies downstream as $M \approx A(x/D)^{\gamma-1}$. Here, x is the axial position, D is the orifice diameter, and $A = \{(\gamma+1)/(\gamma-1)\}^{(\gamma+1)/4}$ is a constant whose value is ≈3. Similarly, it can be shown that the local pressure is related to the Mach number as $P/P_0 \approx \{(\gamma-1)M^2/2\}^{\gamma/(1-\gamma)}$. Consequently, the pressure must drop as the Mach number increases, generally below P_I. However, sooner or later, a transition must be made to P_I, and this adjustment is made via shock waves. Extending from the orifice, the waves form a complex pattern of oblique shocks known as a shock barrel, which terminates in a normal shock known as a Mach disk. The pressure ratio across the normal shock is $P_I/P \approx 2\gamma M^2/(\gamma+1)$, and the Mach number at the shock is $M = B(P_I/P_0)^{(1-\gamma)/2}$. Here, $B = \{2\gamma/(\gamma+1)\}^{(\gamma-1)/2}\{2/(\gamma-1)\}^{\gamma/2}$. Combining these results, the position x_M of the Mach disk may then be found as $x_M/D = C(P_I/P_0)^{-1/2}$. Here, $C = (A/B)^{1/(1-\gamma)}$ is a constant whose value is ≈0.7. The expansion should ideally be continued into the low-pressure chamber without loss in velocity. To achieve this, the Mach disk is pierced with a sharp conical orifice or skimmer. With careful design, the skimmer can attach a conical oblique shock that links the outer flow to the Mach disk while allowing a shock-free expansion of the inner flow into the vacuum chamber. In most systems, the main constraint is that the intermediate pump has sufficient capacity to pull the Mach disk back to the skimmer when a large increase in ion flux is obtained.

C. Miniaturization

Dimensional scaling implies that a reduction in the input orifice size D can allow shorter interface lengths x_M for the same pressure ratio P_I/P_0. Since the maximum flow rate is $Q \approx 0.44\ a_0 D^2\ \mathrm{m}^3/\mathrm{s}$, where a_0 is the sound velocity at atmospheric pressure, a reduction in D should allow smaller interfaces pumped by lower capacity pumps. However, several points deserve consideration. First, for a given ion density in the spray plume, the ion signal is proportional to Q, and hence, the sensitivity will be correspondingly decreased. Second, the presence of a viscous boundary layer will be more significant with smaller orifices, and consequently, it may be difficult to achieve sonic speed at the entrance to the intermediate chamber. In this case, the expansion will be subsonic, losing the desired sensitivity enhancement. Third, the difficulties of constructing a vacuum-tight interface with an optimally shaped skimmer using MEMS processes are formidable. Here, we therefore adopt a simpler approach of using a capillary outlet, which is unlikely to provide a shock-free second-stage expansion. Despite this, we show that recognizable and readily interpreted ESI-MS spectra can be obtained.

III. MEMS ESI-MS System

In this Section, we introduce the MEMS-based ESI-MS system and give a brief overview of component fabrication and functionality.

A. System Overview

Fig. 1(b) shows the MEMS-based ESI-MS system demonstrated here. No attempt has been made to produce a fully integrated system, although this is clearly the eventual aim, and all experiments required additional test equipment. The MEMS components used (here shown in gray) are a nanospray ion source, a vacuum interface, and a quadrupole mass filter. The vacuum chamber, pumps, valves, and gauges are all conventional. However, this approach allows ion generation, ion introduction, and mass filtering, all to be carried out using

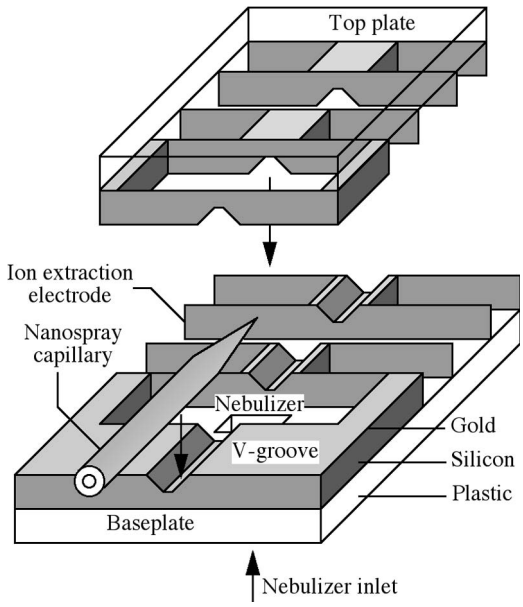

Fig. 3. Overall construction of MEMS nanospray ion source consisting of a nanospray capillary mounted between two silicon MEMS parts that combine together to form ion-extraction electrodes and gas-flow channels for a concentric nebulizer.

batch-fabricated silicon devices that are packaged as interchangeable modules.

B. Nanospray Ion Source

The source is a nanospray ion gun, previously described in [55]. The gun is constructed from two dies, fabricated using a silicon-on-plastic technology that forms a set of discrete Si parts on an SU-8 epoxy resist base. Fig. 3 shows the overall arrangement. The SU-8 is photopatterned to define the overall die outline and an inlet for a nebulizer gas. The silicon layer is etched twice, first using crystal plane etching to form a V-groove mount for a nanospray capillary and other orifices, and second, using DRIE to define an ion-extraction electrode and the flow channel for a coaxial pneumatic nebulizer.

The base-plate and top-plate dies are fabricated together on 100-mm-diameter bulk silicon wafers. KOH etching is first used to form V-grooves in the front side, using an oxide surface mask. The wafer is then turned over, and the rear side is coated with a 300-μm-thick layer of SU-8, which is exposed and developed to form the patterned plastic base. The wafer is turned over again, and a Cr/Au layer is deposited over the grooved surface. This layer is patterned with the electrode layout by wet etching, using electrically deposited Shipley Eagle photoresist. A single-chamber multiplex inductively coupled plasma etcher (Surface Technology Systems, Newport, Wales) operating a cyclic etch based on SF_6 and C_4F_8 (the Bosch process) is then used to transfer the electrodes into the silicon, using the Au as a hard mask and as a subsequent contact layer. After processing, the parts are snapped out of the wafer. The base-plate and top-plate dies are stacked together to form an optical bench that holds the capillary in precise alignment with the ion-extraction electrode. Fig. 4(a) shows a scanning electron microscope (SEM) view of a base-plate with a nanospray capillary mounted in the V-groove, and Fig. 4(b) shows an optical-microscope view of a unit with the top plate now in place. The assembly is mounted on a small printed circuit board (PCB), and electrical connections are made to the electrodes.

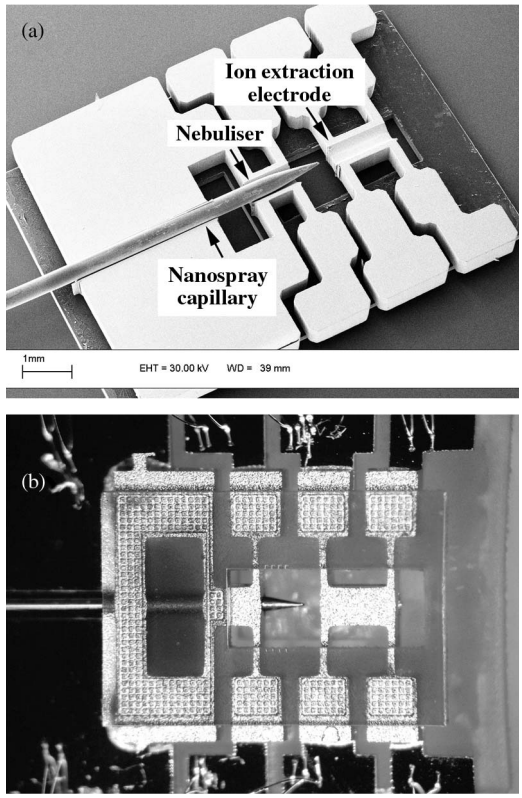

Fig. 4. (a) SEM image of the bottom plate of the nanospray ion source, showing a nanospray capillary mounted in an alignment V-groove on a silicon chip in front of the lower half of an ion-extraction electrode. (b) Photograph of the completed source with the top plate in place, when the electrode halves have been combined together.

C. MEMS Vacuum Interface

The vacuum interface is constructed from two silicon dies attached to a stainless-steel flange. Fig. 5 shows the overall arrangement. The outer die carries features defining an input capillary, an intermediate chamber, and an internal electrostatic lens, while the inner die carries an output capillary, flow channels, and gas ports. The flange incorporates conventionally machined channels for pumping that link to threads for connectors. The die size was initially 12 mm $\times$ 8 mm but was later increased to 15 mm $\times$ 11 mm in order to accommodate a larger rim.

The outer die is formed from a BSOI wafer, consisting of a 500-μm-thick device layer, a 4-μm-thick oxide interlayer, and a 500-μm-thick substrate. The device layer (1) is first patterned and etched three times, using oxide and photoresist hard masks, to form a recess of 500 μm in diameter and 300 μm in depth, a contact via, an input capillary, and the die outline. The wafer is then turned over, and the substrate (2) is etched down to the oxide interlayer to define a 500-μm-diameter chamber beneath the capillary, bounded by an electrostatic lens whose contact is brought through the device layer. The oxide is then removed in

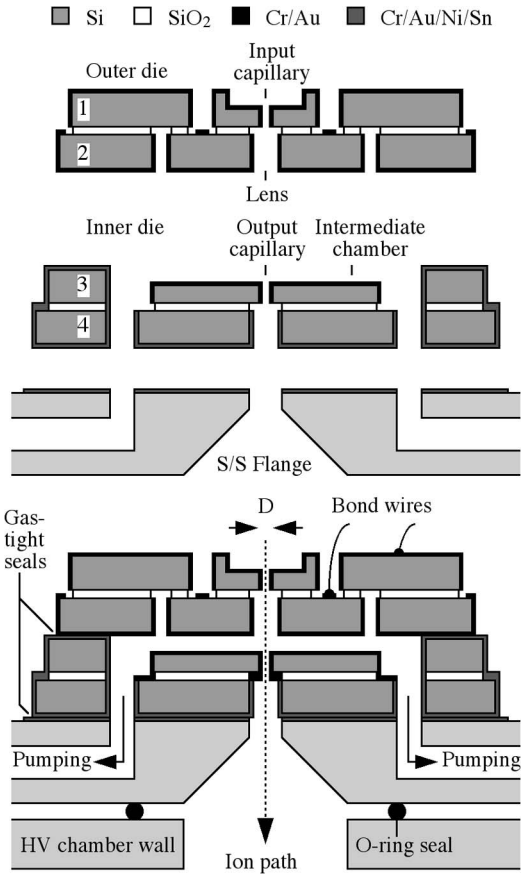

Fig. 5. Overall construction of MEMS vacuum interface. The upper diagram shows the component parts, and the lower diagram shows a complete interface after assembly by stacking. The numbers indicate different layers of silicon; 1 and 2 are device and handle layers in the outer die, while 3 and 4 are device and handle layers in the inner die.

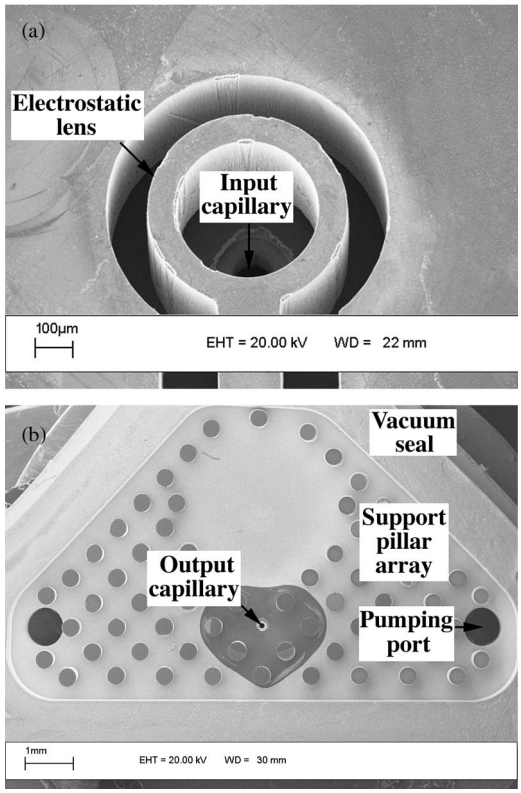

Fig. 6. SEM images of the MEMS vacuum interface showing (a) the internal lens at the center of the outer die, and (b) the support pillars, pumping ports, and output capillary within the recess defined in the inner die.

buffered HF, and both sides of the wafer are coated with 200-nm sputter-deposited Au, using 45-nm Cr for adhesion. Fig. 6(a) shows a SEM view of the inside of the outer die near the input capillary showing the electrostatic lens.

The inner die is also formed from a BSOI wafer, with similar layer thickness. The device layer (3) is first patterned and etched three times to define a 50–100-μm-diameter output capillary surrounded with a deep recess, flow channels, pumping ports, and the die outline. To allow a large pressure difference, internal pillars are used to support the channels, except in regions immediately below the lens and its contact. The substrate (4) is then etched to form extensions of the pumping ports and an enlarged exit. After etching, the wafer is sputter metallized with Cr and Au on both sides. Fig. 6(b) shows a SEM view of the inside of the inner die, showing the output capillary at the center, the gas ports on either side, and supporting pillars (which are removed near the top to provide space for the lens contact). The inner die is then coated with a 1-μm-thick layer of Ni (which acts as a diffusion barrier) and a 10-μm-thick layer of Sn (which acts as a solder) by electroplating, taking care to protect the capillary using photoresist.

The two dies are attached to a vacuum flange, whose outer surface is also sputter coated with Cr/Au and then coated with Ni and Sn by electroplating. Mechanical jigs are used to align the dies over the pumping and venting ports, and the Sn solder is reflowed by heating at 280 °C in forming gas (15% H_2, 85% N_2) to form gas-tight seals. Finally, wirebonds are attached. Since layers 2, 3, and 4 are electrically connected, only layer 1 and the lens can be independently controlled. The output capillary is approximately $x = 800$ μm downstream of the start of the jet expansion. Assuming a capillary diameter of $D = 50$ μm, the Mach disk extends as far as the exit capillary when $x_M/D = 16$.

D. MEMS Quadrupole Mass Filters

Two previously demonstrated MEMS quadrupole mass filters were evaluated. The first is a simple quadrupole fabricated using BSOI material [83], [84]. The second is a quadrupole with a Brubaker prefilter (the use of which can improve ion transmission, particularly in small devices) fabricated using silicon-on-glass [87]. Each type of filter is constructed from two stacked microfabricated dies, each carrying two of the four electrodes required in a quadrupole. Fig. 7(a) compares their construction.

The upper diagram shows the arrangement of a bonded silicon die, which, for the 30-mm-long electrodes, measures ≈ 35 mm $\times$ 6 mm. Both silicon layers are structured using DRIE to form electrodes and rod mounts, and the oxide interlayer provides electrical isolation between the different electrodes. For the 650-μm-diameter electrodes, a device layer thickness of ≈ 105 μm is used, together with a substrate thickness of 400 μm and an oxide-interlayer thickness of 2 μm. The

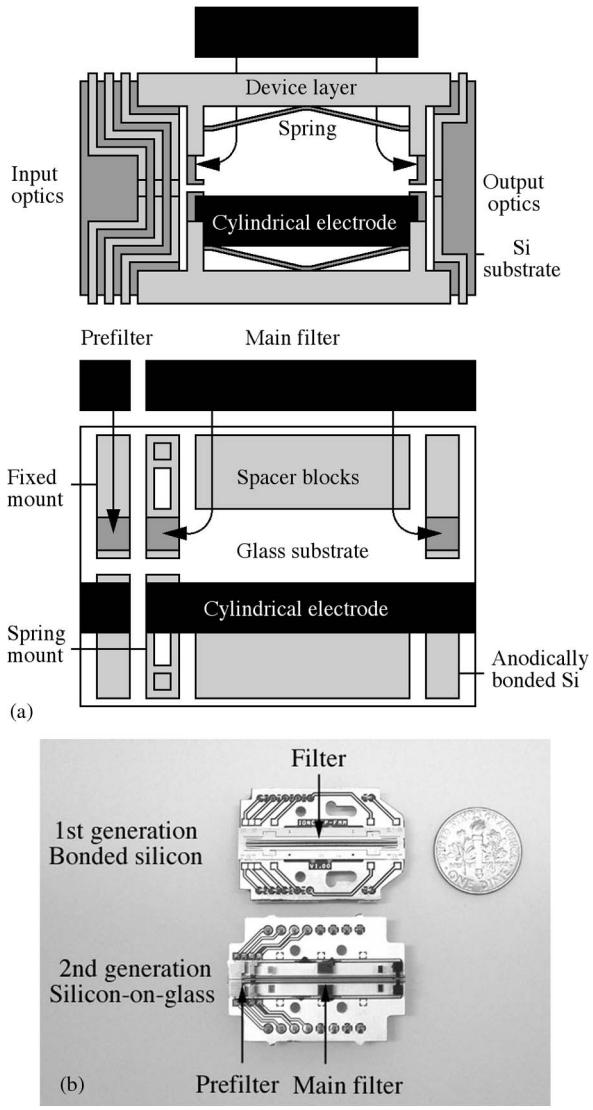

Fig. 7. (a) Die layouts and (b) complete filters in (upper) BSOI and (lower) silicon-on-glass. Each device consists of two stacked microfabricated dies that each provide mounting frames for half of the rods required in a complete quadrupole. The layouts show the method of rod mounting, while the photographs show the filters mounted on small PCBs.

substrate is first etched to form in-plane alignment features and retaining springs for a pair of cylindrical electrodes. The device layer is then etched twice, to form out-of-plane rod alignment features, together with ion optical elements at the entrance and exit of the filter. A three-element electrostatic lens is used at the input, and a single aperture is used at the output.

The lower diagram shows the arrangement of a silicon-on-glass die, which has similar dimensions. Here, silicon parts that have been structured using DRIE are anodically bonded to a glass substrate, which then provides improved electrical isolation. The electrode rods are now arranged in two sections, with a 4-mm-long prefilter preceding the 30-mm-long main filter. The electrodes are now rigidly attached to the silicon mounting blocks. However, to avoid deformation by thermal-expansion mismatch between the electrode rods and the substrate, suspended spring mountings are provided for the main-filter electrodes.

To construct a complete filter, two dies are stacked together back-to-back so that the quadrupole geometry is formed. In the bonded silicon device, the features etched into the device layers also form sets of entrance and exit electrodes containing central pupils. These pupils are, however, both rectangular and relatively small and significantly limit ion transmission [84]. The assembly is then attached to a small PCB and wirebond connections are made to the electrode contacts. In each case, stainless-steel electrode rods are inserted into each die in appropriate locations. Electrodes are inserted after assembly in the bonded silicon device and before assembly in the silicon-on-glass device. Fig. 7(b) shows the completed mass filters of each type.

IV. Experimental Results

In this section, we describe the performance of the nanospray ion source, the transmission of ions and partitioning of the gas flow by the vacuum interface, and the acquisition of mass spectra using the two different quadrupole mass filters.

A. Nanospray Ion Generation

The operation of the MEMS nanospray source was demonstrated using Silica Tapertip capillaries with an outside diameter of 320 μm and an inside diameter of 15 μm (New Objective, Woburn, MA). The nanospray source was movable in all three directions, but the motion of the nanospray capillary was restricted to preset axial adjustment. A solution of 75% water, 20% methanol, and 5% acetic acid was supplied at flow rates in the range of 1–40 μL/h (17–670 nL/min) using a syringe pump (100-CE, KD Scientific Holliston, U.S.). Nebulizing gas (N_2) was introduced to the plenum chamber through a conduit in the aluminum enclosure and a mating hole in the PCB submount. A flow controller was used to set the flow in the range of 2–5 L/min.

Spray was generated using a voltage applied by a custom dc power supply between the capillary and the ion-extraction electrode, with the polarity arranged for positive-ion production. The on-chip electrode allows a stable ion stream to be generated without an MS inlet being present. Electrical isolation is excellent, and the technology can support an on-chip voltage of up to $\approx$1.5 kV. However, much lower voltages are typically required for optimum performance. Using an axial separation of ≈ 500 μm, the threshold voltage and the operating voltage are $\approx$700 and $\approx$850 V, respectively. The precise mechanical alignment between the capillary and electrode ensures that these voltages are repeatable. Fig. 8(a) shows how the total ion current typically varies with applied voltage, using measurements averaged over a 1-min period. A range of liquid flow rates was used, with an axial separation of 450 μm between the capillary and ion-extraction electrode. In each case, the voltage rises rapidly from a threshold voltage that depends mainly on the capillary ID and flow rate. Fig. 8(b) shows the corresponding variation of total ion current with flow rate, at different set voltages, which shows that the current rises quasi-linearly with flow rate until the onset of jet instability. Below this point, the spray was highly stable, and many hours of operation could be obtained without blockage or other failure.

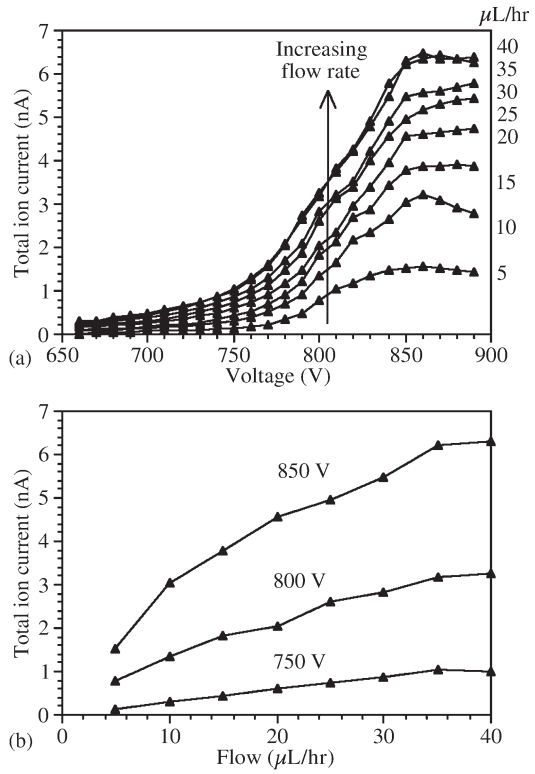

Fig. 8. Variation of electrosprayed ion current with (a) voltage, for different flow rates, and (b) flow rate, at different voltages, for MEMS nanospray source with 15-μm-ID Silica Tapertip capillary.

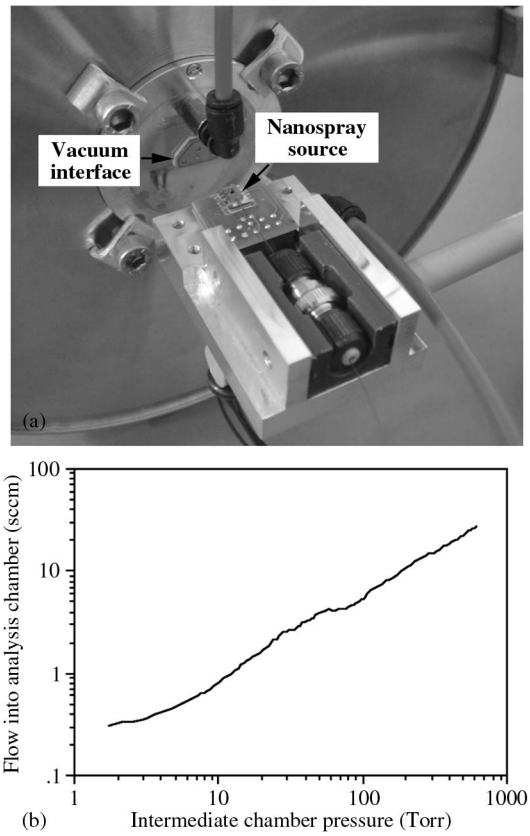

Fig. 9. (a) Nanospray ion source positioned in front of the vacuum interface. A protective cover that would normally conceal the source has been removed. The nanospray chip may be seen immediately in front of a union that connects the analyte feed capillary to the nanospray tip. (b) Variation of the gas flow into the analysis chamber with intermediate-stage pressure.

B. Gas-Load Partitioning

Characterization of the MEMS vacuum interface was performed using a 6-L stainless-steel vacuum chamber pumped by a 250-L/s turbomolecular pump (TV-301 Navigator, Varian S.P.A., Torino, Italy) through a 100-mm-diameter port. Two ISO 200 flanges were used as the end plates of the cylindrical section chamber. One was machined with a central-aperture counterbored to receive a gasket and the vacuum-interface flange, while the other was used for access during experimental setup. A full-range pressure gauge (Pfeiffer Vacuum, Asslar, Germany) and two electrical feedthrough flanges were mounted on ports distributed around the waist of the chamber.

Fig. 9(a) shows the nanospray unit in front of the vacuum chamber. The MEMS component is at the front of the module. To the rear, a metal union connects the spray tip to the supply capillary and is also used to establish a connection to the high-voltage (HV) supply when nonconductive tips are used. The MEMS vacuum interface is at the center of the figure, below an elbow joint that connects the flange to the pumping line. Channels within the flange connect to the pumping ports in the MEMS interface. In later versions, the MEMS vacuum interfaces were mounted on small metal tabs that were more easily interchanged. Vacuum integrity was verified before use by immersing the interface in water and checking for leaks other than through the inlet and exit capillaries when a positive gas pressure was applied via the pumping line.

A Pirani gauge (MicroPirani 925C, MKS Instruments, Boulder, CO) was used to monitor the pressure in the pumping line. However, due to the low conductance of the pumping ports in the MEMS interface, this is not necessarily an accurate measure of the pressure in the internal cavity. Either a 4.8-L/min diaphragm pump (N84.4 ANDC, KNF Neuberger, Freiburg, Germany) or a 110-L/min scroll pump (SH-110, Varian, Lexington, MA) were used to pump the interface. The base pressures achieved in the vacuum manifold were 15 and 2 torr, respectively. A throttling valve or a variable air bleed close to the pump was used to vary the pressure as necessary.

The gas flow into the analysis chamber is dictated by the speed of the selected pump and the maximum tolerable operating pressure. It is the purpose of the vacuum interface to partition the total gas flow passing through the inlet from the atmosphere. The turbomolecular pump used with the test system is relatively large, and as a result, a substantial fraction of the total gas load can be allowed into the analysis chamber. However, the development of a complete miniaturized ESI-MS system would undoubtedly require a significantly smaller high-vacuum pump and removal of much more of the gas load at the intermediate stage.

The range of gas-load partitioning that can be achieved by the MEMS vacuum interface was characterized by measuring the pressure in the analysis chamber as the interface pumping speed was gradually decreased (either by throttling the pump or by increasing the air bleed). Rather than plot the analysis-chamber pressure, which depends on the speed of the turbomolecular pump, the volumetric gas flow into the analysis

chamber (calculated by multiplying the measured pressure in the chamber by the known pumping speed) has been plotted against the intermediate-stage pressure, as shown in Fig. 9(b). A quasi-linear relationship is observed, except at low intermediate pressures when the flow levels off at a value of 0.3 standard cubic centimeters per minute (sccm). If the inlet capillary is blocked with a rubber pad, the flow into the analysis chamber immediately drops from 0.3 to 0.07 sccm, indicating that most of this residual gas load is due to the flow through the inlet, rather than leaks and outgassing.

The design of the MEMS interface is simple, and its internal cavity is very small. Nevertheless, this component is effective in partitioning the gas flow through the inlet. Despite the brittle nature of silicon, there was no difficulty sustaining a pressure difference between atmosphere on one side of the vacuum interface and high vacuum on the other. Although vacuum-packaged silicon devices have been available for many years, this result represents the first demonstration of a differentially pumped MEMS component.

As the ultimate goal of this work is to produce a miniaturized integrated instrument, some consideration of the possible pumping arrangements is worthwhile. Several small lightweight diaphragm and rotary-vane pumps that would be suitable for pumping the interface are commercially available. These would typically be able to achieve an intermediate-stage pressure of 5–30 torr. If the intermediate-stage pressure were 15 torr, for example, a turbo pump with a pumping speed of approximately 16 L/s would be able to maintain the analysis chamber at 1×10^{-3} torr. Many modern turbo pumps incorporate multiple drag stages that allow foreline pressures of as high as 30 torr. Consequently, another small diaphragm or rotary-vane pump would be suitable as the backup pump for the turbo pump.

C. Ion Transfer Into Vacuum

Ion transmission into the HV analysis chamber was monitored by a channeltron electron multiplier (Magnum, Photonis USA Inc., Sturbridge, MA) mounted behind a 4-mm aperture in an aluminum plate, ≈5 cm from the vacuum interface. Pulses from the channeltron were filtered using a discriminator and counted for periods ranging from 30 ms to 10 s. Each pulse is initiated when a cascade of secondary electrons is generated by the collision of a charged particle with surface of the channeltron input horn. However, the measured count rate cannot be equated directly to ion flux entering the chamber as the detection efficiency of the channeltron is significantly less than unity. Not all the ions striking the input result in a pulse that can be counted, and it cannot be guaranteed that all of the ions are scavenged by the HV applied to its input. Consequently, several measurements at high intermediate-stage pressure were repeated with the channeltron, and its shield was replaced by a large Faraday plate, biased at −18 V to attract ions entering the vacuum chamber. The absolute ion transmission was determined by dividing the drain current measured with a picoammeter (Keithley 6485, Keithley Instruments Inc., Cleveland, OH) by the elementary charge, which was then used to calibrate the data obtained with the channeltron.

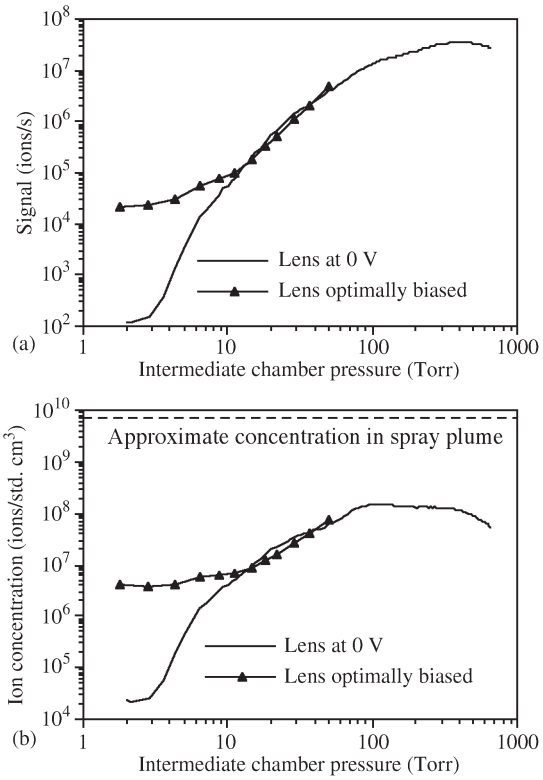

Fig. 10. (a) Variation of the ion transmission into the analysis chamber with intermediate-stage pressure. (b) Variation of the ion concentration in the gas flow with intermediate-stage pressure, compared with the approximate concentration in the spray plume.

The calibration procedure assumes that there are no multiply charged ions present (a doubly charged ion, for example, would register as a single pulse when detected by the channeltron but would contribute two elementary charges to the current flowing from the Faraday plate). This assumption is supported by an investigation of water cluster ions with a wide range of masses, formed by spraying acidic aqueous solutions, which has shown that only singly charged cluster ions are produced [96].

Fig. 10(a) shows the variation of absolute ion transmission with the intermediate chamber pressure. At intermediate pressures in the range 2–350 torr, the ion-transmission approximately reflects the gas flow into the analysis chamber. Given that the ions are entrained in the gas flow and all the components of the vacuum interface are held at 0 V, it might be anticipated that the concentration of ions passing into the analysis chamber would be constant. However, this is evidently not the case. Whereas the gas flow varies by two orders of magnitude, the ion transmission varies by six orders. The absolute ion concentration can be calculated by dividing the ion transmission by the gas flow, as shown in Fig. 10(b), together with the approximate concentration of ions in the spray plume (calculated using the spray current and the nebulizing gas flow). The maximum ion concentration entering the analysis chamber is 2% of the concentration in the spray plume. Neutralization on the metallized walls of the inlet and exit capillaries and the internal structures within the MEMS interface is likely to be responsible for this depletion of the ion concentration. However, collisions with the walls are less likely at higher pressures when the mean free path is short, and the flow through the interface is dominated

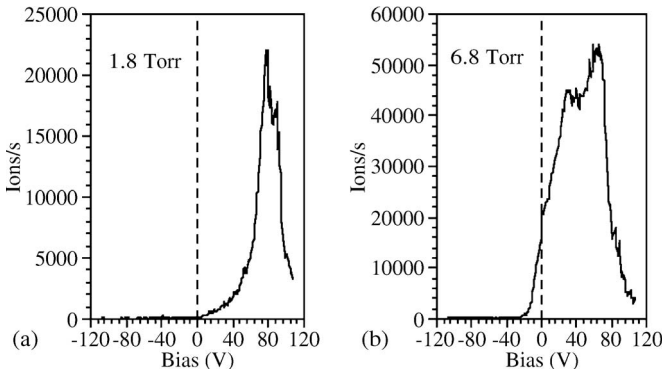

Fig. 11. Response of the ion transmission to the bias applied to the vacuum-interface internal lens at intermediate-stage pressures of 1.8 and 6.8 torr.

by viscous drag. As the pressure in the intermediate stage is reduced, the mean free path increases, and collisions with the walls become more likely.

D. Ion Concentration Using Internal Optics

This interpretation is reinforced by the behavior observed when a voltage was applied to the internal lens contained in the MEMS vacuum interface. Fig. 11 shows the variation of ion transmission with bias (incremented in 1-V steps) at two different intermediate pressures (1.8 and 6.8 torr). At lower pressure, the ion transmission increases from a negligible value at 0 V to over 20 000 ions/s at +80 V. Focusing is also seen at higher pressure, but there is only a threefold enhancement over the value at 0 V. The optimum bias voltage was determined for intermediate pressures in the range of 2–50 torr, and the corresponding ion-transmission measurements are shown in Fig. 10(a) and (b). At low pressures, the free-jet expansion extends far into the internal cavity, and ions that would otherwise be lost through collisions with the walls can be focused into the exit capillary. As the intermediate pressure increases, electrostatic focusing becomes less effective since the free-jet expansion retracts toward the inlet, and the mean free path in the stagnant gas reduces.

Above approximately 380 torr, the ion transmission levels off and then actually decreases. This behavior is in excellent agreement with the transition from choked flow to pressure-dependent flow in the inlet capillary, which occurs at a pressure $P_i = P_0\{2/(\gamma+1)\}^{\gamma/(\gamma-1)}$ (≈400 torr for $\gamma = 7/5$). At higher intermediate pressures, the flow of gas and entrained ions becomes proportional to the pressure difference across the inlet capillary.

E. ESI-MS Using a Simple Quadrupole

To demonstrate ESI-MS, the free-standing channeltron was removed from the vacuum chamber and replaced with a bespoke alignment jig containing a MEMS quadrupole filter with an input aperture plate and a channeltron detector. The quadrupole filter was operated at 6.5 MHz, biased at 0 V, and driven with ramped dc and ac voltages whose relative values were chosen to place the scan line near the tip of the first stability zone. To improve ion coupling, the vacuum interface was biased at +10–20 V, which accelerates the ions toward the mass filter and thereby reduces the angular divergence of the beam.

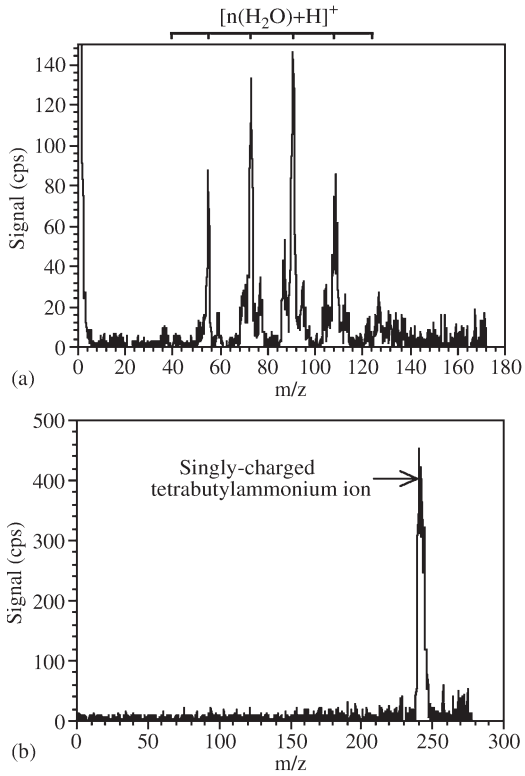

Fig. 12. (a) ESI-MS spectrum of a solution of 75% water, 20% methanol, and 5% acetic acid. The prominent peaks correspond to $[\mathrm{n(H_2O)} + \mathrm{H}]^+$. (b) ESI-MS spectrum of a solution of 150 μg/ml TBAH in a 50 : 50 mixture of methanol and water.

A possible complication of the experimental setup is that large charged droplets are able to follow straight-line trajectories from the nanospray capillary tip directly into the input of the channeltron as the nanospray source, vacuum-interface apertures, mass filter, and channeltron detector are all positioned along the same common axis. However, the background ion count observed when recording the spectra is always very low, indicating that droplets are not present.

Fig. 12(a) shows a mass spectrum recorded while spraying a solution of 75% water, 20% methanol, and 5% acetic acid. Multiple scans were averaged to improve the signal-to-noise ratio, and the total acquisition period for each data point was 0.795 s. The interval between each data point is 0.2 m/z units. Three well-known series of singly charged cluster ions can be identified [1], [96], although several of the peaks can only be seen clearly on expansion of the vertical axis. The prominent series at $m/z = 37, 55, 73, 91, 109,$ and 127 correspond to $[\mathrm{n(H_2O)} + \mathrm{H}]^+$. A minor series at $m/z = 51, 69, 87, 105,$ and 123 corresponds to $[\mathrm{n(H_2O)} + \mathrm{CH_3OH} + \mathrm{H}]^+$, and a further minor series at $m/z = 59, 77, 95, 113,$ and 131 can be assigned as $[\mathrm{n(H_2O)} + \mathrm{Na}]^+$. Such sodium ion adducts arise from trace impurities in the solvent and are frequently observed in ESI-MS spectra.

A solution of water, methanol, and acetic acid was chosen for initial testing primarily because the yield of ions is likely to be

high. However, of equal importance is the propensity for water cluster ion formation as the distribution of these clusters helps to characterize the nanospray ion source and any processes occurring in the vacuum interface. In general, cluster ion formation is undesirable. Large clusters can lie beyond the mass range of the analyzer, whereas smaller clusters complicate the mass spectrum. Incomplete desolvation in the spray plume is not usually a concern as a high flow rate of nebulizing gas, which is often heated, ensures efficient desolvation in conventional pneumatically assisted electrospray. In some instruments, off-axis sampling of the spray plume helps to preferentially select lighter more completely desolvated ions. The lower flow rates used in nanospray result in a smaller initial droplet size, and desolvation is consequently achieved more readily. Of greater concern is the condensation of ions and free solvent molecules during the initial adiabatic free-jet expansion into the first vacuum stage. Typically, this can be reduced by using a gas curtain or counterflow of nitrogen to prevent neutral solvent molecules from passing through the inlet aperture. Heating the inlet aperture also reduces the likelihood that the cooling during expansion will be sufficient to allow condensation with any remaining solvent molecules.

Despite on-axis sampling and the absence of heating, a curtain gas, or a counterflow of nitrogen, only small clusters can be identified in Fig. 12(a). The highest mass ion contains seven water molecules, and the most prominent ion contains just five. It is not clear whether these clusters result from incomplete desolvation in the spray plume or from condensation during the first expansion. This result is in stark contrast to the spectrum reported by Ledman and Fox [96]. These authors used a high solvent flow rate, low drying gas flow rate, and low source temperature, and omitted any counterflow gas to promote water cluster ion formation. As a result, they were able to observe an extensive series of clusters up to $m/z = 1900$. The limited series of peaks seen here suggests, first, that efficient desolvation is achieved by the nanospray ion source, and second, that any larger clusters formed in the initial expansion are reheated by scattering before passing into the analysis chamber.

It is unlikely that the mass filter suffers from any mass discrimination that would abruptly terminate the cluster series at $m/z = 131$. Previous work with an electron-impact ion source has shown that mass spectra with the correct cracking pattern intensities in the range $m/z = 0{-}400$ can be recorded using the MEMS mass filter [83], [84].

Fig. 12(b) shows a mass spectrum recorded while spraying a solution of 150 μg/ml tetrabutylammonium hydroxide (TBAH) in a 50 : 50 mixture of methanol and water. Again, a relatively high ion yield is expected, as TBAH is a strong base and almost completely ionized in solution. This spectrum was acquired using a relatively low U/V value and a total signal acquisition period of 0.405 s per data point. A single peak at $m/z = 242$, corresponding to the tetrabutylammonium ion, can be seen. There is no evidence of impurities or fragmentation products. These results demonstrate that mass spectra can be obtained using embryonic MEMS components, even when many of the precautions commonly taken to improve spectral quality are omitted.

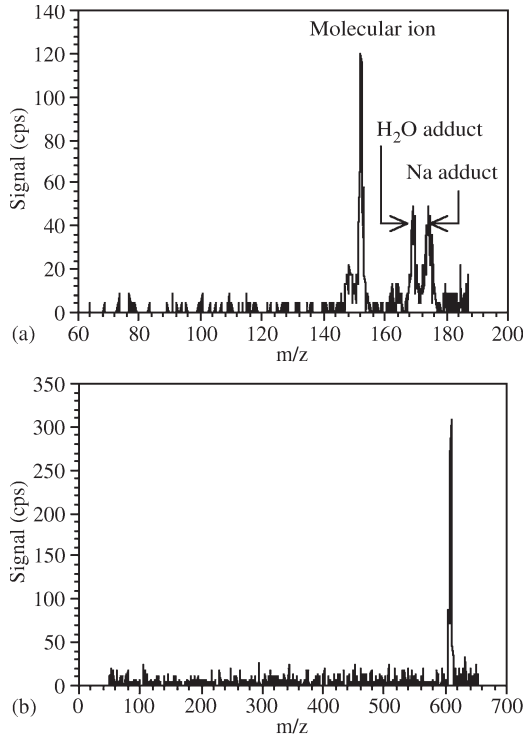

Fig. 13. ESI-MS spectrum of (a) acetaminophen (paracetamol) and (b) reserpine obtained using the silicon-on-glass quadrupole.

F. ESI-MS Using a Quadrupole With a Prefilter

Exchanging the simple bonded silicon quadrupole with the second-generation silicon-on-glass device, which incorporated a prefilter, yielded significant improvement in the signal level, mass resolution, and mass range. This enhanced performance allowed analysis of analytes that are more challenging than TBAH. Fig. 13(a) shows a mass spectrum recorded while spraying a solution of 1-mg/ml acetaminophen (paracetamol) in a 50 : 50 mixture of acetonitrile and water with 0.1% formic acid. Multiple scans were averaged, and the total signal acquisition period per data point was 0.225 s. The molecular ion can be identified at $m/z = 152$. Additionally, there are smaller peaks at $m/z = 170$ and $m/z = 174$, corresponding to H_2O and Na^+ adducts, respectively. A mass spectrum recorded while spraying a solution of 1-mg/ml reserpine in a 50 : 50 mixture of acetonitrile and water with 0.1% formic acid is shown in Fig. 13(b). In this case, the acquisition period was 0.309 s per data point, and the molecular ion can be identified at $m/z = 609$.

For comparison with the earlier results, a spectrum of TBAH was also recorded, using an acquisition period of 0.15 s per data point. These data are shown in Fig. 14(a), together with a spectrum recorded using a commercial ESI-MS system that has been rescaled for comparison [Fig. 14(b)]. The resolution achieved with the silicon-on-glass quadrupole ($m/\Delta m = 270$ at full-width at half-maximum) is clearly much higher than that achieved with the bonded silicon device and compares favorably with the performance of the commercial system in that the spectra are qualitatively very similar. It is important to point out, however, that the commercial instrument is able to maintain unit resolution at high mass and delivers a much higher signal level. While the first and second isotope peaks are

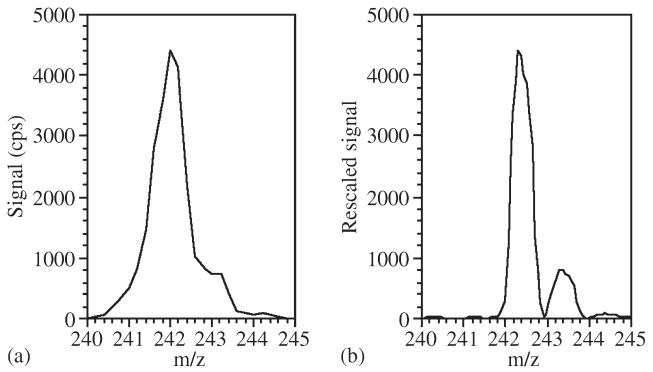

Fig. 14. Mass spectra of TBAH near the tetrabutylammonium molecular ion peak obtained using (a) the MEMS ESI-MS system with a silicon-on-glass quadrupole and (b) a Waters ZQ ESI-MS.

not completely resolved in Fig. 14(a), they can nevertheless be identified as distinct shoulders.

V. Conclusion

We have demonstrated a nanospray-ionization MS system whose ion source, vacuum interface, and mass filter are all constructed as separate silicon MEMS. Clearly, further work is required to improve sensitivity, mass range, and mass resolution. However, even the relatively simple components used in these initial experiments have allowed readily interpretable mass spectra to be obtained. It has been demonstrated that performance enhancements can follow from systematic improvements of each MEMS component (for example, by using a quadrupole filter equipped with a Brubaker prefilter). The use of microfabrication technology allows key features such as precise mechanical alignment, complex electrode arrangements, and vacuum seals to be achieved on a small scale at low cost. As a result, the components are compact, batch fabricated, interchangeable, and potentially disposable. This demonstration represents a further step in the miniaturization of MSs using MEMS.

Acknowledgment

The authors would like to thank A. Finlay, A. Malcolm, M.-A. Schwab, Dr. H. Zou, Dr. M. Bardwell, and Dr. A. Lipson for their contributions.

References

[1] M. Yamashita and J. B. Fenn, "Electrospray ion source. Another variation on the free-jet theme," *J. Phys. Chem.*, vol. 88, no. 20, pp. 4451–4459, Sep. 1984.

[2] M. G. Ikonomou, A. T. Blades, and P. Kebarle, "Investigations of the electrospray interface for liquid chromatography/mass spectrometry," *Anal. Chem.*, vol. 62, no. 9, pp. 957–967, May 1990.

[3] D. C. Gale and R. D. Smith, "Small volume and low flow-rate electrospray ionization mass spectrometry of aqueous samples," *Rapid Commun. Mass Spectrom.*, vol. 7, no. 11, pp. 1017–1021, Nov. 1993.

[4] M. Wilm and M. Mann, "Electrospray and Taylor-cone theory, Dole's beam of macromolecules at last?" *Int. J. Mass Spectrom. Ion Process.*, vol. 136, no. 2/3, pp. 167–180, Sep. 1994.

[5] G. A. Valaskovic, "Long-lived metallized tips for nanoliter electrospray mass spectrometry," *J. Amer. Soc. Mass Spectrom.*, vol. 7, no. 12, pp. 1270–1272, Dec. 1996.

[6] M. Wilm and M. Mann, "Analytical properties of the nanoelectrospray ion source," *Anal. Chem.*, vol. 68, no. 1, pp. 1–8, Jan. 1996.

[7] J. C. Hannis and D. C. Muddiman, "Nanoelectrospray mass spectrometry using non-metallized, tapered ($50 \rightarrow 10$ μm) fused silica capillaries," *Rapid Commun. Mass Spectrom.*, vol. 12, no. 8, pp. 443–448, Apr. 1998.

[8] R. Juraschek, T. Dulcks, and M. Karas, "Nanoelectrospray—More than just a minimized-flow electrospray interface," *J. Amer. Soc. Mass Spectrom.*, vol. 10, pp. 300–308, Apr. 1999.

[9] K. Oswatitsch and W. Rothstein, "Flow pattern in a converging-diverging nozzle," NASA, Washington, DC, Rep. NACA-TM-1215, 1949.

[10] P. L. Owen and C. K. Thornhill, The Flow in an Axially Symmetric Supersonic Jet From a Nearly Sonic Orifice Into a Vacuum, Sep. 1948, Aeronautical Research Council Reports and Memorabilia 2616.

[11] A. Kantrowitz and J. Grey, "A high intensity source for the molecular beam. Part I. Theoretical," *Rev. Sci. Instrum.*, vol. 22, no. 5, pp. 328–332, May 1951.

[12] G. B. Kistiakowsky and W. P. Slichter, "A high intensity source for the molecular beam. Part II. Experimental," *Rev. Sci. Instrum.*, vol. 22, no. 5, pp. 333–337, May 1951.

[13] K. Bier and O. Hagena, "Influence of shock waves on the generation of high intensity molecular beams by nozzles," in *Rarefied Gas Dynamics*, vol. I, J. A. Lauermann, Ed. New York: Academic, 1963, pp. 478–496.

[14] J. B. Fenn and J. Deckers, "Molecular beams from nozzle sources," in *Rarefied Gas Dynamics*, vol. I, J. A. Lauermann, Ed. New York: Academic, 1963, pp. 497–515.

[15] R. Campargue, "High intensity supersonic molecular beam apparatus," *Rev. Sci. Instrum.*, vol. 35, no. 1, pp. 111–112, Jan. 1964.

[16] J. B. Anderson and J. B. Fenn, "Velocity distributions in molecular beams from nozzle sources," *Phys. Fluids*, vol. 8, no. 5, pp. 780–787, May 1965.

[17] R. Campargue, "Progress in overexpanded supersonic jets and skimmed molecular beams in free-jet zones of silence," *J. Phys. Chem.*, vol. 88, no. 20, pp. 4466–4474, Apr. 1984.

[18] J. B. Anderson, "Molecular beams from nozzle sources," in *Molecular Beams and Low Density Gasdynamics*, R. P. Wegener, Ed. New York: Marcel Dekker, 1974, pp. 1–91.

[19] G. Sanna and G. Tomassetti, *Introduction to Molecular Beams Gas Dynamics*. London, U.K.: Imperial College Press, Sep. 2005.

[20] H. Ashkenas and F. S. Sherman, "The structure and utilization of supersonic free jets in low density wind tunnels," in *Rarefied Gas Dynamics*, vol. II, J. H. De Leeuw, Ed. New York: Academic, 1966, pp. 84–105.

[21] R. S. Houk, V. A. Fassel, G. D. Flesch, H. J. Svec, A. L. Gray, and C. E. Taylor, "Inductively coupled argon plasma as an ion source for mass spectrometric determination of trace elements," *Anal. Chem.*, vol. 52, pp. 2283–2289, Dec. 1980.

[22] J. A. Olivares and R. S. Houk, "Ion sampling for inductively coupled plasma mass spectrometry," *Anal. Chem.*, vol. 57, no. 13, pp. 2674–2679, Nov. 1985.

[23] D. J. Douglas and J. B. French, "Gas dynamics of the inductively coupled plasma mass spectrometry interface," *J. Anal. Atom. Spectrom.*, vol. 3, no. 6, pp. 743–747, Sep. 1988.

[24] A. L. Gray, "Visual observation of shock waves in an inductively coupled plasma mass spectrometry expansion stage," *J. Anal. Atom. Spectrom.*, vol. 4, pp. 371–373, Jun. 1989.

[25] T. N. Olney, T. N. Chen, and D. J. Douglas, "Gas dynamics of the ICP-MS interface: Impact pressure probe measurements of gas flow profiles," *J. Anal. Atom. Spectrom.*, vol. 14, pp. 9–17, Jan. 1999.

[26] J. H. Macedone, A. A. Mills, and P. B. Farnsworth, "Optical measurements of ion trajectories through the vacuum interface of the inductively coupled plasma mass spectrometer," *Appl. Spectrosc.*, vol. 58, no. 4, pp. 463–467, Apr. 2004.

[27] C. M. Whitehouse, R. N. Dreyer, M. Yamashita, and J. B. Fenn, "Electrospray interface for liquid chromatographs and mass spectrometers," *Anal. Chem.*, vol. 57, no. 3, pp. 675–679, Mar. 1985.

[28] A. P. Bruins, T. C. Covey, and J. D. Henion, "Ion spray interface for combined liquid chromatography/atmospheric pressure ionization mass spectrometry," *Anal. Chem.*, vol. 59, no. 22, pp. 2642–2646, Nov. 1987.

[29] K. L. Duffin, T. Wachs, and J. D. Henion, "Atmospheric-pressure ion-sampling system for liquid-chromatography mass-spectrometry analyses on a benchtop mass-spectrometer," *Anal. Chem.*, vol. 64, no. 1, pp. 61–68, Jan. 1992.

[30] A. V. Mordehai, G. Hopfgartner, T. G. Huggins, and J. D. Henion, "Atmospheric-pressure ionization interface for a bench-top quadrupole ion trap," *Rapid Commun. Mass Spectrom.*, vol. 6, no. 8, pp. 508–516, Aug. 1992.

[31] A. V. Morhedai and J. D. Henion, "A novel differentially pumped design for atmospheric pressure ionization-ion trap mass spectrometry," *Rapid Commun. Mass Spectrom.*, vol. 7, no. 3, pp. 205–209, Apr. 1993.

[32] A. V. Tolmachev, I. V. Chernushevich, A. F. Dodonov, and K. G. Standing, "A collision focusing ion guide for coupling an atmospheric pressure ion source to a mass spectrometer," *Nucl. Instrum. Methods Phys. Res. B, Beam Interact. Mater. At.*, vol. 124, no. 1, pp. 112–119, Apr. 1997.

[33] B. C. Cha, M. Blades, and D. J. Douglas, "An interface with a linear quadrupole ion guide for an electrospray-ion trap mass spectrometer system," *Anal. Chem.*, vol. 72, no. 22, pp. 5647–5654, Oct. 2000.

[34] P. V. Bondarenko and R. D. MacFarlane, "A new electrospray-ionization time-of-flight mass spectrometer with electrostatic wire ion guide," *Int. J. Mass Spectrom. Ion Process.*, vol. 160, no. 1–3, pp. 241–258, Jan. 1997.

[35] R. Zhang, L. T. Molina, and M. J. Molina, "Development of an electrostatic ion guide in chemical ionization mass spectrometry," *Rev. Sci. Instrum.*, vol. 69, no. 11, pp. 4002–4003, Nov. 1998.

[36] Y. Takada, M. Sakairi, and Y. Ose, "Electrostatic ion guide using double cylindrical electrode for atmospheric pressure ionization mass spectrometry," *Rev. Sci. Instrum.*, vol. 67, no. 6, pp. 2139–2141, Jun. 1996.

[37] K. Giles, S. D. Pringle, K. R. Worthington, D. Little, J. L. Wildgoose, and R. H. Bateman, "Applications of a travelling wave-based radio-frequency-only stacked ring ion guide," *Rapid Commun. Mass Spectrom.*, vol. 18, no. 20, pp. 2401–2414, Sep. 2004.

[38] B. B. Schneider, V. I. Baranov, H. Javaheri, and T. R. Covey, "Particle discriminator interface for nanoflow ESI-MS," *J. Amer. Soc. Mass Spectrom.*, vol. 14, no. 11, pp. 1236–1246, Nov. 2003.

[39] J. Abian, "The coupling of gas and liquid chromatography with mass spectrometry," *J. Mass Spectrom.*, vol. 34, pp. 157–168, Mar. 1999.

[40] T. R. Covey, B. A. Thomson, and B. B. Schneider, "Atmospheric pressure ion sources," *Mass Spectrom. Rev.*, vol. 28, no. 6, pp. 870–897, Jul. 2009.

[41] R. Ramsey and J. Ramsey, "Generating electrospray from microchip devices using electroosmotic pumping," *Anal. Chem.*, vol. 69, no. 13, pp. 1174–1178, Mar. 1997.

[42] D. Figeys, Y. B. Ning, and R. Aebersold, "A microfabricated device for rapid protein identification by microelectrospray ion trap mass spectrometry," *Anal. Chem.*, vol. 69, no. 16, pp. 3153–3160, Aug. 1997.

[43] A. Desai, Y. C. Tai, M. T. Davis, and T. D. Lee, "A MEMS electrospray nozzle for mass spectrometry," in *Proc. Int. Conf. Solid State Sens. Actuators TRANSDUCERS*, May 1997, pp. 927–930.

[44] B. Zhang, H. Liu, B. L. Karger, and F. Foret, "Microfabricated devices for capillary electrophoresis-electrospray mass spectrometry," *Anal. Chem.*, vol. 71, no. 15, pp. 3258–3264, Jun. 1999.

[45] L. Licklider, X. Q. Wang, A. Desai, Y. C. Tai, and T. D. Lee, "A micromachined chip-based electrospray source for mass spectrometry," *Anal. Chem.*, vol. 72, no. 2, pp. 367–375, Jan. 2000.

[46] C.-H. Yuan and J. Shiea, "Sequential electrospray analysis using sharp-tip channels fabricated on a plastic chip," *Anal. Chem.*, vol. 73, no. 6, pp. 1080–1083, Mar. 2001.

[47] J. Kameoka, R. Orth, D. Czaplewski, T. Wachs, and H. G. Craighead, "An electrospray ionization source for integration with microfluidics," *Anal. Chem.*, vol. 74, no. 22, pp. 5897–5901, Nov. 2002.

[48] S. Arscott, S. Le Gac, C. Druon, P. Tabourier, and C. Rolando, "A planar on-chip micro-nib interface for NanoESI-MS microfluidic applications," *J. Micromech. Microeng.*, vol. 14, no. 2, pp. 310–316, Feb. 2004.

[49] B. Legrand, A. E. Ashcroft, L. Buchaillot, and S. Arscott, "SOI-based nanoelectrospray emitter tips for mass spectrometry: A coupled MEMS and microfluidic design," *J. Micromech. Microeng.*, vol. 17, no. 3, pp. 509–514, Mar. 2007.

[50] Q. Xue, F. Foret, Y. M. Dunayevskiy, P. M. Zavracky, N. E. McGruer, and B. L. Karger, "Multichannel microchip electrospray mass spectrometry," *Anal. Chem.*, vol. 69, no. 3, pp. 426–430, Feb. 1997.

[51] H. Liu, C. Felten, Q. Xue, B. Zhang, P. Jedrzejewski, B. L. Karger, and F. Foret, "Development of multichannel devices with an array of electrospray tips for high-throughput mass spectrometry," *Anal. Chem.*, vol. 72, no. 14, pp. 3303–3310, Jul. 2000.

[52] G. A. Schultz, T. N. Corso, S. J. Prosser, and S. Zhang, "A fully integrated monolithic microchip electrospray device for mass spectrometry," *Anal. Chem.*, vol. 72, no. 17, pp. 4058–4063, Aug. 2000.

[53] K. Tang, Y. Lin, D. W. Matson, T. Kim, and R. D. Smith, "Generation of multiple electrosprays using microfabricated emitter arrays for improved mass spectrometric sensitivity," *Anal. Chem.*, vol. 73, no. 8, pp. 1658–1663, Apr. 2001.

[54] A. K. Sen, J. Darabi, and D. R. Knapp, "Design, fabrication and test of a microfluidic nebulizer chip for desorption electrospray ionization mass spectrometry," *Sens. Actuators B, Chem.*, vol. 137, no. 2, pp. 789–796, Apr. 2009.

[55] R. R. A. Syms, H. Zou, M. Bardwell, and M.-A. Schwab, "Microengineered alignment bench for a nanospray ionisation source," *J. Micromech. Microeng.*, vol. 17, no. 8, pp. 1567–1574, Aug. 2007.

[56] J. M. Lazar, J. Grym, and F. Foret, "Microfabricated devices: A new sample introduction approach to mass spectrometry," *Mass Spectrom. Rev.*, vol. 25, no. 4, pp. 573–594, Jul./Aug. 2006.

[57] F. Foret and P. Kusy, "Microdevices in mass spectrometry," *Eur. J. Mass. Spectrom.*, vol. 13, no. 1, pp. 41–33, Feb. 2007.

[58] S. Koster and E. Verpoorte, "A decade of microfluidic analysis coupled with electrospray mass spectrometry: An overview," *Lab. Chip*, vol. 7, no. 11, pp. 1394–1412, Sep. 2007.

[59] T. Sikanen, S. Franssila, T. J. Kauppila, R. Kostianinen, T. Kotiaho, and R. A. Ketola, "Microchip technology in mass spectrometry," *Mass Spectrom. Rev.*, vol. 29, no. 3, pp. 351–391, May/Jun. 2009.

[60] C. Freidhoff, "Mass spectrograph on a chip," in *Proc. IEEE Aerosp. Conf.*, Aspen, CO, Feb. 1997, vol. 3, p. 32.

[61] C. B. Freidhoff, R. M. Young, S. Sriram, T. T. Braggins, T. W. O'Keefe, J. D. Adam, H. C. Nathanson, R. R. A. Syms, T. J. Tate, M. M. Ahmad, S. Taylor, and J. Tunstall, "Chemical sensing using nonoptical microelectromechanical systems," *J. Vac. Sci. Technol. A, Vac. Surf. Films*, vol. 17, no. 4, pp. 2300–2307, Mar./Apr. 1999.

[62] N. Sillon and R. Baptist, "Micromachined mass spectrometer," *Sens. Actuators B, Chem.*, vol. 83, no. 1–3, pp. 129–137, Mar. 2002.

[63] P. Siebert, G. Petzold, A. Hellenbart, and J. Müller, "Surface microstructure/miniature mass spectrometer: Processing and applications," *Appl. Phys. A, Solids Surf.*, vol. 67, no. 2, pp. 155–160, Aug. 1998.

[64] J.-P. Hauschild, E. Wapelhorst, and J. Müller, "Mass spectra measured by a fully integrated MEMS mass spectrometer," *Int. J. Mass Spectrom.*, vol. 264, no. 1, pp. 53–60, May 2007.

[65] J. Hauschild, E. Wapelhorst, and J. Müller, "The novel synchronous ion shield mass analyzer," *J. Mass Spectrom.*, vol. 44, no. 9, pp. 1330–1337, Aug. 2009.

[66] H. J. Yoon, J. H. Kim, E. S. Choi, S. S. Yang, and K. W. Jung, "Fabrication of a novel micro time-of-flight mass spectrometer," *Sens. Actuators A, Phys.*, vol. 97/98, pp. 441–447, Apr. 2002.

[67] J. S. Hwang, S. W. Park, J. B. Cho, K. S. Oh, S. S. Yang, S. Lee, K. H. Koh, and K. W. Jung, "The micro mass spectrometer with a carbon nanostructure ion source," in *Proc. 1st IEEE Int. Conf. Nano/Micro Eng. Molec. Syst.*, Zuhai, China, Jan. 2006, pp. 1220–1223.

[68] J. Fox, R. Saini, K. Tsui, and G. Verbeck, "Microelectromechanical system assembled ion optics: An advance to miniaturization and assembly of electron and ion optics," *Rev. Sci. Instrum.*, vol. 80, no. 9, p. 093 302, Sep. 2009.

[69] E. Wapelhorst, J.-P. Hauschild, and J. Müller, "Complex MEMS: A fully integrated TOF micro mass spectrometer," *Sens. Actuators A, Phys.*, vol. 138, no. 1, pp. 22–27, Apr. 2007.

[70] R. G. Brewer, R. G. Devoe, and R. Kallenbach, "Planar ion microtraps," *Phys. Rev. A, Gen. Phys.*, vol. 46, no. 11, pp. R6 781–R6 784, Dec. 1992.

[71] E. R. Badman, R. C. Johnson, W. R. Plass, and R. G. Cooks, "A miniature cylindrical quadrupole ion trap: Simulation and experiment," *Anal. Chem.*, vol. 70, no. 23, pp. 4896–4901, Dec. 1998.

[72] O. Kornienko, P. T. A. Reilly, W. B. Whitten, and J. M. Ramsey, "Micro ion trap mass spectrometry," *Rapid Commun. Mass Spectrom.*, vol. 13, no. 1, pp. 50–53, Jan. 1999.

[73] M. G. Blain, L. S. Riter, D. Cruz, D. E. Austin, G. X. Wu, W. R. Plass, and R. G. Cooks, "Towards the hand-held mass spectrometer: Design considerations, simulation, and fabrication of micrometer-scaled cylindrical ion traps," *Int. J. Mass Spectrom.*, vol. 236, no. 1–3, pp. 91–104, Aug. 2004.

[74] S. Pau, C. S. Pai, Y. L. Low, J. Moxom, P. T. A. Reilly, W. B. Whitten, and J. M. Ramsey, "Microfabricated quadrupole ion trap for mass spectrometer applications," *Phys. Rev. Lett.*, vol. 96, no. 12, pp. 120 801-1–120 801-4, Mar. 2006.

[75] A. Chaudhary, F. H. W. van Amerom, and R. T. Short, "Development of microfabricated cylindrical ion trap mass spectrometer arrays," *J. Microelectromech. Syst.*, vol. 18, no. 2, pp. 442–448, Apr. 2009.

[76] M. J. Madsen, W. K. Hensinger, D. Stick, J. A. Ratschuk, and C. Monroe, "Planar ion trap geometry for microfabrication," *Appl. Phys. B, Photophys. Laser Chem.*, vol. 78, no. 5, pp. 639–651, Mar. 2004.

[77] M. Brownnutt, G. Wilpers, P. Gill, R. C. Thompson, and A. G. Sinclair, "Monolithic microfabricated ion trap chip design for scaleable quantum processors," *New J. Phys.*, vol. 8, no. 10, p. 232, Oct. 2006.

[78] M. Debatin, M. Kröner, J. Mikosch, S. Trippel, N. Morrison, M. Reetz-Lamour, P. Woias, R. Wester, and M. Weidmüller, "Planar multipole ion trap," *Phys. Rev. A, Gen. Phys.*, vol. 77, no. 3, p. 033 422, Mar. 2008.

[79] M. Yu, M. Fico, S. Kothari, Z. Ouyang, and W. J. Chappell, "Polymer-based ion trap chemical sensor," *IEEE Sensors J.*, vol. 6, no. 6, pp. 1429–1434, Dec. 2006.

[80] M. Fico, J. Maas, S. A. Smith, A. B. Costa, Z. Ouyang, W. J. Chappell, and R. G. Cooks, "Circular arrays of polymer-based miniature rectilinear ion traps," *Analyst*, vol. 134, no. 7, pp. 1338–1347, Apr. 2009.
[81] R. R. A. Syms, T. J. Tate, M. M. Ahmad, and S. Taylor, "Design of a microengineered quadrupole electrostatic lens," *IEEE Trans. Electron Devices*, vol. 45, no. 11, pp. 2304–2311, Nov. 1998.
[82] S. Taylor, J. J. Tunstall, J. H. Leck, R. Tindall, P. Julian, J. Batey, R. R. A. Syms, T. J. Tate, and M. M. Ahmad, "Performance improvements for a miniature quadrupole with a micromachined mass filter," *Vacuum*, vol. 53, no. 1/2, pp. 203–206, May 1999.
[83] M. Geear, R. R. A. Syms, S. Wright, and A. S. Holmes, "Monolithic MEMS quadrupole mass spectrometers by deep silicon etching," *J. Microelectromech. Syst.*, vol. 14, no. 5, pp. 1156–1166, Oct. 2005.
[84] S. Wright, R. R. A. Syms, S. O'Prey, G. Hong, and A. S. Holmes, "Comparison of ion coupling strategies for a microengineered quadrupole mass spectrometer," *J. Amer. Soc. Mass Spectrom.*, vol. 20, no. 1, pp. 146–156, Jan. 2009.
[85] A. Malcolm, S. Wright, R. R. A. Syms, N. Dash, M.-A. Schwab, and A. Finlay, "Miniature mass spectrometer systems based on a microengineered quadrupole filter," *Anal. Chem.*, vol. 82, no. 5, pp. 1751–1758, Mar. 2010.
[86] L. F. Velasquez-Garcia, K. Cheung, and A. L. Akinwande, "An application of 3-D MEMS packaging: Out-of-plane quadrupole mass filters," *J. Microelectromech. Syst.*, vol. 17, no. 6, pp. 1430–1438, Dec. 2008.
[87] S. Wright, S. O'Prey, R. R. A. Syms, G. Hong, and A. S. Holmes, "Microfabricated quadrupole mass spectrometer with a Brubaker prefilter," *J. Microelectromech. Syst.*, vol. 19, no. 2, pp. 325–337, Apr. 2010.
[88] K. Cheung, L. F. Velasquez-Garcia, and A. I. Akinwande, "First principles optimization of mass produced microscaled linear quadrupoles for operation in higher stability regions," in *Proc. 20th IEEE Int. Vac. Nanoelectron. Conf.*, 2007, pp. 214–215.
[89] K. Cheung, L. F. Velasquez-Garcia, and A. I. Akinwande, "High-performance MEMS square electrode quadrupole mass filters for chip-scale mass spectrometry," in *Proc. MEMS*, Hong Kong, Jan. 2010, pp. 867–870.
[90] B. Brkic, N. France, A. T. Clare, C. J. Sutcliffe, P. R. Chalker, and S. Taylor, "Development of quadrupole mass spectrometers using rapid prototyping technology," *J. Amer. Soc. Mass Spectrom.*, vol. 20, no. 7, pp. 1359–1365, Apr. 2009.
[91] A. T. Clare, L. Gao, B. Brkic, P. R. Chalker, and S. Taylor, "Linear ion trap fabricated using rapid manufacturing technology," *J. Amer. Soc. Mass Spectrom.*, vol. 21, no. 2, pp. 317–322, Feb. 2010.
[92] E. R. Badman and R. G. Cooks, "Special feature: Perspective—Miniature mass analysers," *J. Mass Spectrom.*, vol. 35, pp. 659–671, Jun. 2000.
[93] T. Nohmi and T. Miyagashi, "Future mass from miniaturized mass spectrometry to micro mass spectrometry," *J. Mass Spectrom. Soc. Jpn.*, vol. 51, no. 1, pp. 54–66, Jan. 2003.
[94] Z. Ouyang and R. G. Cooks, "Miniature mass spectrometers," *Annu. Rev. Anal. Chem.*, vol. 2, pp. 10.1–10.28, Jul. 2009.
[95] R. R. A. Syms, "Advances in microfabricated mass filters," *Anal. Bioanal. Chem.*, vol. 393, no. 2, pp. 427–429, Jan. 2009.
[96] D. W. Ledman and R. O. Fox, "Water cluster calibration reduces mass error in electrospray ionization mass spectrometry of proteins," *J. Amer. Soc. Mass Spectrom.*, vol. 8, no. 11, pp. 1158–1164, Nov. 1997.

Steven Wright was born in London, U.K., in 1970. He received the B.Sc. degree in chemistry and the Ph.D. degree in physical chemistry from the University of Southampton, Southampton, U.K., in 1992 and 1996, respectively.

Between 1995 and 2000, he was a Postdoctoral Researcher at the Fritz Haber Institute, Berlin, Germany, Odense University, Odense, Denmark, the University of Duisburg–Essen, Germany, and the University of Liverpool, Liverpool, U.K. His research interests were in the field of chemical and photochemical reactions on single crystal surfaces. In 2000, he was with Applied Materials U.K., where he was involved in the development of ion-implant systems. He has been with Microsaic Systems Ltd., Surrey, U.K., since 2003 and has been its Mass Spectrometry Manager since 2006.

Richard R. A. Syms (SM'02) received the B.A. degree in engineering science and the D.Phil. degree (on volume holographic optical elements) from Worcester College, Oxford University, Oxford, U.K., in 1979 and 1982, respectively.

He has been the Head of the Optical and Semiconductor Devices Group, Department of Electrical and Electronic Engineering, Imperial College London, London, U.K., since 1992 and Professor of Microsystems Technology since 1996. He has published over 150 journal papers and two books on holography, guided-wave optics, and microengineering. Most recently, he has been developing electrical MEMS such as microconnectors, RF probes for magnetic resonance imaging, and miniature quadrupole mass spectrometers; optical MEMS devices such as alignment devices, variable optical attenuators, and tunable lasers; and 3-D self-assembling microstructures. He cofounded the MEMS spin-out company Microsaic Systems Ltd., Surrey, U.K., in 2001. He is currently an Associate Editor of the JOURNAL OF MICROELECTROMECHANICAL SYSTEMS.

Richard Moseley was born in Munich, Germany, in 1975. He received the B.Sc. degree in physics and chemistry of materials from the University of Durham, Durham, U.K., in 1996, and the Ph.D. degree in device physics from the University of Cambridge, Cambridge, U.K., in 2000.

His research interests were in the field of nonequilibrium superconductivity. In 2000, he was with Agilent Technologies, working at the company's R&D sites in Ipswich, U.K. and Turin, Italy. There, he was involved in the development of semiconductor lasers for fiber-optic transceiver applications. He has been with Microsaic Systems Ltd., Surrey, U.K., since 2003 and became its Devices Manager in 2006. His work has involved developing various MEMS devices for mass-spectrometry and RF applications, including an RF switch and a self-assembled vertical inductor.

Dr. Moseley is a member of the Institute of Physics and the European Microwave Association.

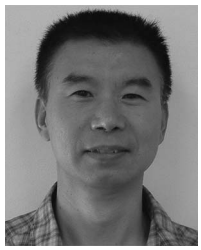

Guodong Hong was born in Shandong, China, in 1964. He received the B.Eng. and M.Eng. degrees in material engineering from Shandong University, Jinan, China, in 1984 and 1989, respectively, and the Ph.D. degree in mechanical engineering from Tsinghua University, Beijing, China, in 1998.

He was a Research Fellow at Nanyang Technological University, Singapore, between 1998 and 2000. He was a Research Associate at Imperial College London, London, U.K., between 2000 and 2004. He has been with Microsaic Systems Ltd., Surrey, U.K., since 2005, where he is currently a Product Development Engineer for miniature mass-spectrometer design and development.

Shane O'Prey received the B.Sc. degree in pure physics and the Ph.D. degree in physics from Queen's University Belfast, Belfast, U.K., in 1996 and 2002, respectively. The focus of his Ph.D. research was the design and utilization of a system that used surface plasmon resonance effects to investigate the dielectric function of thin-film metals and high-temperature superconducting materials at liquid-nitrogen temperatures.

After several years with Intel Ireland as a Yield Engineer investigating the root cause of inline defects, he returned to research at Polight Technologies, a Cambridge-based start-up company, developing glass materials for holographic data storage. He has been with Microsaic Systems Ltd., Surrey, U.K., since 2005 as a Development Engineer, working extensively on the design and manufacture of MEMS mass-spectrometer devices.

William E. Boxford was born in Northampton, U.K., in 1980. He received the M.Sci. degree in chemistry from the University of Bristol, Bristol, U.K., in 2002, and the Ph.D. degree in chemistry from the University of York, York, U.K., in 2008.

His research focused on the fundamental physics of exotic ions in the gas-phase using a variety of experimental and theoretical methods. He has been with Microsaic Systems Ltd., Surrey, U.K. since 2006, where he has played an integral role in the design, development, and applications of mass spectrometer systems based on novel MEMS technology.

Neil Dash was born in Bristol, U.K., in 1979. He received the B.Sc. degree in chemistry and the Ph.D. degree in physical chemistry from the University of Wales, Swansea, U.K., in 2000 and 2004, respectively.

Between 2004 and 2005, he was a Postdoctoral Researcher at the University of Wales, Swansea. His Ph.D. and postdoctoral work research interests were in the field of fast flow glow discharges, monitoring reactions, and excited state behavior using mass spectrometry. Since 2005, he has been with Microsaic Systems Ltd., Surrey, U.K., where he became a Senior Engineer in 2009.

Peter Edwards was born in Wales, U.K., in 1956. He received the B.Sc. degree in engineering from Kingston University, Kingston upon Thames, U.K.

Between 1978 and 1986, he was in the U.K. and U.S. working in the field of robotics and flight simulation. He was elected as a Chartered Engineer in 1985. He joined Applied Materials U.K. Ltd., in 1987 and, as Engineering Director and subsequently Business Unit Director, he led the development of several generations of award winning ion-implantation equipment for advanced semiconductor fabrication. He has been with Microsaic Systems Ltd., Surrey, U.K., since 2007 as Head of Research and Development.